The study of the influence of Jahn-Teller coupling and low symmetry strain on the anomalous electron paramagnetic resonance spectrum of titanium(III) doped $CsAl(SO_4)_2 \cdot 12H_2O$

Philip L. W. Tregenna-Piggott, Christopher J. Noble, and John R. Pilbrow

Citation: The Journal of Chemical Physics **113**, 3289 (2000); doi: 10.1063/1.1287281

View online: https://doi.org/10.1063/1.1287281

View Table of Contents: http://aip.scitation.org/toc/jcp/113/8

Published by the American Institute of Physics

The study of the influence of Jahn-Teller coupling and low symmetry strain on the anomalous electron paramagnetic resonance spectrum of titanium(III) doped $CsAl(SO_4)_2 \cdot 12H_2O$

Philip L. W. Tregenna-Piggott[a)]
Department of Chemistry, University of Bern, Freiestrasse 3, Bern 9, CH-3000, Switzerland

Christopher J. Noble[a),b)] and John R. Pilbrow
Department of Physics, Monash University, Clayton, Victoria 3168 Australia

(Received 9 May 2000; accepted 30 May 2000)

The controversial EPR spectrum of titanium(III) as an impurity in cesium aluminum sulphate alum has been re-examined using conventional CW- and a novel pulsed-EPR technique, which monitors the nutation frequency as a function of field. The CW-spectra display a high degree of structure, which is interpreted as arising from chemically distinct titanium(III) species. The two-dimensional nutation spectrum maps the $g_\parallel$ vs $g_\perp$ relation from just one crystal orientation, and to far greater precision than available from CW-EPR. This novel technique shows that the origin of the linewidths observed for some of the EPR lines is inhomogeneous broadening, the nature of which can be described adequately only in the two-dimensional nutation spectrum. Calculations of $g_\parallel$ vs $g_\perp$ have been undertaken by numerical diagonalization of the vibronic Hamiltonian. It is found that the relationship between $g_\parallel$ and $g_\perp$ can be modeled only by assuming that the titanium(III) ions are subject to both dynamic Jahn-Teller coupling and low symmetry strain. Furthermore, it is shown that the calculated $g_\parallel$ vs $g_\perp$ relation is strongly dependent upon the nature of the vibronic interaction assumed. An excellent reproduction of the experimental data is obtained, using parameters consistent with those employed to model the susceptibility data of the isostructural cesium titanium sulphate alum. © *2000 American Institute of Physics.* [S0021-9606(00)02832-4]

I. INTRODUCTION

The interpretation of the anomalous EPR spectrum of titanium(III) doped $CsAl(SO_4)_2 \cdot 12H_2O$ (Cs[Al:Ti]SH) has been one of the most contentious topics in the theory of the electronic structure of transition metal ions, with numerous models posited.[1–6] The titanium(III) ion substitutes for aluminum(III), which lies on a site of trigonal (S_6) symmetry in a cubic ($Pa3$) lattice, with the threefold axes of the tervalent cations directed along the [111] directions of the crystal. The spectrum obtained for each titanium(III) site consists of a number of lines as first reported by Woonton and MacKinnon.[1] As only one transition is normally expected, the problem has been to account for the additional structure. These authors identified three prominent resonances, with the [111] direction of the crystal aligned with the external field, which they assigned to three chemically distinct titanium(III) species. Soon afterwards a similar spectrum was reported by Shing and Walsh,[4] who proposed an elaborate model in which the transitions observed occur between the levels of a Γ_8 ground state split by a small trigonal field. This explanation was based on the supposition that the ${}^2T_{2g}(O_h)$ ground term is subject to a strong dynamic Jahn-Teller effect, the nature of which leads to an almost complete quenching of the trigonal field. This model attracted considerable attention at the time, as it was thought to constitute a textbook example of the phenomenon of Ham-quenching.[7] However, this rather fantastic explanation has subsequently been rejected as untenable, on the basis of the relative magnitudes of the ligand field and Jahn-Teller interactions implied.[5,6,8] There is now overwhelming evidence to suggest that the trigonal field is very large, and of a sign such that the orbital doublet lies below the orbital singlet.[9,10] The resulting ${}^2E_g$ ground term is subject to Jahn-Teller and spin–orbit coupling and a delicate balance between these two interactions has shown to be responsible for the anomalous magnetic properties of $CsTi(SO_4)_2 \cdot 12H_2O$ and its magnetically dilute analogs.[5,6,8,11]

Recent work by Dubicki and Riley[5] has demonstrated that the additional structure observed in the EPR spectra of Cs[Al:Ti]SH can be explained assuming a distribution of chemically distinct species, subject to varying amounts of low symmetry strain. Furthermore, these authors showed that the g values are very sensitive to the strength of the strain interaction, and the parameters associated with the vibronic Hamiltonian in general. Therefore, the accurate and precise determination of the g values is essential to understand the nature of the vibronic interaction. However, the controversy surrounding the interpretation of the EPR spectrum of this system has arisen, in part, because the information available from the CW-EPR spectra is limited. For some of the EPR lines, $g_\perp$ cannot be determined directly by CW-EPR, owing to the very low value of $g_\perp$.[1,4] Furthermore, when a [111] face of the crystal is directed away from the external field,

a)Authors to whom correspondence should be addressed.
b)Present address: Centre for Magnetic Resonance, University of Queensland, St. Lucia, Queensland 4072 Australia.

some of the lines exhibit considerable broadening and lose any meaningful intensity.[1,4]

This work presents new EPR data, which confirm the interpretation that the multiline spectrum results as a consequence of chemically distinct titanium(III) species. Our work utilises a new pulsed-EPR technique, which affords the precise determination of the principal g values of all the EPR lines without the need to change the crystal orientation. It is shown that the origin of the large linewidths observed for some of the CW-EPR lines is inhomogeneous broadening; and that the $g_\parallel$ vs $g_\perp$ relation can be reproduced only by assuming a rather specific vibronic coupling model.

II. EXPERIMENT

A. Sample preparation

Crystals used in this study were grown by cocrystallization of $CsM^{III}(SO_4)_2 \cdot 12H_2O$, where M^{III} is Al, Ga or In (CsAlSH, CsGaSH, CsInSH) with either $CsTi(SO_4)_2 \cdot 12H_2O$ (CsTiSH) or $CsV(SO_4)_2 \cdot 12H_2O$ (CsVSH) in H_2SO_4 (1 M).[6] In some instances, a very small amount of $CsCr(SO_4)_2 \cdot 12H_2O$ was added to assist alignment of the crystal in the external magnetic field.

The crystal denoted Cs[Ga:Ti]SH_B weighed 0.28 g, and was prepared by a slow deposition method described previously.[12] Spectra from this crystal were obtained using the EPR facility at the Grenoble high magnetic field laboratory. All the other crystals were prepared by a fast deposition method, allowing a hot solution containing a mixture of the salts, and deoxygenated using the freeze–pump–thaw technique, to cool to room temperature. Crystals obtained by this method formed quickly, and the size and quality of the crystals were variable. For the Cs[Al:Ti]SH samples, good quality EPR crystals were obtained by dissolving ≈3 g of solid in 80 ml of hot H_2SO_4 (1 M). The crystals selected for EPR experiments from the resulting yield weighed between 2.2 and 11.4 mg.

EPR spectra were recorded from crystals containing variable amounts of titanium(III). The percentage of titanium(III) given in the text corresponds to that present in solution as a percentage of the total tervalent cation concentration. Elemental analysis, using the ICP–AES technique, on batches of crystals formed from the 2% and 1% solutions, revealed average titanium(III) concentrations of ca. 0.8% and 0.2%, respectively. The exact amount of titanium(III) in the crystals used for the EPR experiments will, however, depend on whether the crystal in question was amongst the first or last to crystallize from the mother liquor. The crystals had well defined [111] faces, which allowed them to be mounted on a sample rod such that the applied field was in a {110} plane. All orientations of the magnetic field in this plane could then be achieved by rotation of the sample holder. Measurements were performed with the sample in an atmosphere of helium to assist heat conduction.

B. Instrumental details

X-band EPR spectra were recorded on a Bruker ESP380e spectrometer at the Department of Physics, Monash University, in conjunction with a dielectric *X*-band resonator and on Oxford Instruments CF 935 liquid helium cryostat. Samples were sealed under an atmosphere of helium, to assist heat conduction. The spectra were recorded at the lowest temperature, approximately 1.7 K, which could be achieved while pumping on the helium reservoir. The Bruker dielectric probehead was used for both the CW- and pulsed-EPR experiments. *X*-band spectra were also recorded on a Bruker ELEXSYS spectrometer at the Department of Chemistry, University of Bern, in conjunction with an Oxford instruments ESR 910 cryostat, and either a ER 4122 SHQ or a ER 4116 DM *X*-band resonator. Two small apertures were bored at the base at 60 mm from the base of the sample tube, to allow helium gas to pass over the sample. The spectra were obtained at the base temperature of the cryostat, 1.7(1) K, which was estimated using a Cernox sensor. Identical spectra were obtained from both *X*-band spectrometers. *S*-band spectra were obtained at the Center of Magnetic Resonance, University of Queensland, using a Bruker ESP300e spectrometer in combination with a Bruker split-ring resonator and an Oxford Instruments CF 935 liquid helium cryostat. *W*-band spectra were obtained at the Grenoble High Magnetic Field Laboratory; the experimental setup has been described in detail previously.[13]

C. The 2D nutation spectrum

The principal g values for some of the EPR lines cannot be established directly from CW-EPR, owing to their low g values and weak intensity, as we shall show in Sec. IV. In view of this problem, we have developed a new pulsed-EPR sequence, which is able to determine precisely the principal g values of all the EPR lines, without the need to reorient the crystal. The technique is based upon the principal of simultaneously measuring the absorbance and the nutation frequency (precession frequency of the spin packets in the rotating frame of reference) as a function of field.

In the instance of axial g values, and neglecting off-resonance effects, the nutation frequency is given by[14]

$$\omega_{\mathrm{nut}} = 2\pi g_1 \beta \mathbf{B}_1 / h, \tag{1}$$

where

$$g_1 = \sqrt{\left(\frac{g_\perp g_\parallel}{g}\right)^2 \cos^2\alpha + g_\perp^2 \sin^2\alpha} \tag{2}$$

and

$$g = \sqrt{g_\parallel^2 \cos^2\theta + g_\perp^2 \sin^2\theta}. \tag{3}$$

B_1 is the microwave magnetic field, θ is the angle between the static magnetic field and the principal direction of the axial g matrix, and α is the orientation of the B_1 field vector in the plane perpendicular to B_0. If $\theta = 0°$, $g_1 = g_\perp$, and $g = g_\parallel$; the resonant field position yields $g_\parallel$ and the nutation frequency is proportional to $g_\perp$. This is the basis for simultaneously measuring $g_\parallel$ and $g_\perp$.

It has been shown recently, that it is possible, using nutation spectroscopy, to measure accurately small g values that are difficult or impossible to obtain with standard CW EPR techniques.[14] Several echo detected nutation experiments have been proposed. The simplest experiment consists of a primary echo sequence where the first pulse is replaced by a high turn angle (HTA) pulse of variable length

(HTA-τ-π-τ-echo).[15] The echo amplitude is then monitored as a function of the HTA pulse length. Alternatively, the turn angle of the first pulse is kept at $\pi/2$ and the second pulse is incremented ($\pi/2$-τ-HTA-τ-echo).[16] In another variation, both pulses can be incremented so that a ratio of 1:2 is maintained between the length of the two pulses (HTA-τ-HTA-τ-echo).[17] Stoll *et al.* have recently introduced a novel pulse sequence, phase-inverted echo-amplitude detected nutation (PEANUT), which was found to have a number of advantages over the previously described experiments.[18] The PEANUT sequence, $(\pi/2)_x$-τ-$(\mathrm{HTA})_x(\mathrm{HTA})_{-x}$-$\tau$-echo, has two HTA pulses with opposing phases and lengths t and $T-t$. The total length of the two HTA pulses remains constant during the experiment as t is incremented. The principal advantages of the PEANUT sequence are: the refocusing of B_1 inhomogeneities, the constant length of the pulse sequence (which results in nutation spectra that are free from relaxation broadening) and the selectivity that can be achieved by adjusting the initial $\pi/2$ pulse.

The pulse sequence used in this study is another variation of the primary echo experiment. Both pulses are HTA pulses but in contrast to the third example (HTA-τ-HTA-τ-echo)[17] given above, the length of the pulses are incremented and decremented, with lengths t and $T-t$, as in the PEANUT experiment. This type of incrementation scheme has also been used for free evolution periods in ESEEM experiments.[19] The length of the experiment therefore remains constant and the nutation spectra are not broadened by relaxation. The relaxation time still limits the length of the pulse sequence, however. Other features of the PEANUT sequence,[14,18] such as the refocusing of B_1 inhomogeneities, are not maintained in this pulse sequence.

This pulse-sequence was developed since the selectivity offered by the initial $\pi/2$ pulse in the PEANUT sequence is actually seen to be a disadvantage for the present system under study. The spectrum consists of a broad continuous distribution of g values, and hence nutation frequencies; this means that portions of the spectrum will only be selected for a given nominal $\pi/2$ pulse. This will result in a distorted spectrum. We wish to recover information regarding this distribution of g values and therefore we argue that the pulse sequence used in this study, which does not have pulses with a nominal turn angle, is more appropriate. Our two-pulse technique is also simpler to use and results in a stronger echo and a better signal to noise ratio. The full technical details of this experiment shall be published in a future paper.

III. THEORY

A. The vibronic Hamiltonian

The crystal field has cubic and trigonal components giving rise to a ground orbital doublet and higher-lying orbital singlet.[9] Dubicki and Riley have performed exact calculations on the linear ${}^2T_2 \otimes e$ Jahn-Teller coupling interaction in trigonal symmetry, incorporating spin–orbit coupling and off-diagonal trigonal field terms from the higher lying cubic ${}^2E$ term.[5] These authors calculated the ground state g values for strains of different symmetries and concluded that the fine structure observed in the EPR spectrum of Cs[Al:Ti]SH must arise as a consequence of low symmetry perturbations. Concurrently with their work, a detailed account of the magnetic properties of CsTiSH and Cs[Ga:Ti]SH was provided by employing a similar calculation but restricting the electronic basis to the ${}^2E_g$ trigonal ground term only.[6,11] This is justified on account of the large trigonal and cubic fields, as borne out by a comparison of the results of the calculations, with those of Dubicki and Riley. We employ the same approximation here as the number of parameters required to model the data is greatly reduced, and the general features of the EPR spectra are satisfactorily reproduced.

The Hamiltonian describing the vibronic interaction between the ${}^2E_g$ ground term and a spectrum of E_g phonons, in the presence of a small low symmetry crystal field, may be written as

$$\begin{aligned} H = {} & E_0\tau + \sum_i (1/2\mu_i)[\mathbf{P}_{\theta_i}^2 + \mathbf{P}_{\epsilon_i}^2 + \mu_i^2\omega_i^2(\mathbf{Q}_{\theta_i}^2 + \mathbf{Q}_{\epsilon_i}^2)]\tau \\ & + V_i[\mathbf{Q}_{\theta_i}\mathbf{U}_\theta + \mathbf{Q}_{\epsilon_i}\mathbf{U}_\epsilon] + e_\theta\mathbf{U}_\theta + e_\epsilon\mathbf{U}_\epsilon + \lambda\mathbf{L}\cdot\mathbf{S} \\ & + B\beta(k\mathbf{L} + 2\mathbf{S}), \end{aligned} \tag{4}$$

where E_0 is the energy of the doubly degenerate electronic state resulting from the cubic and trigonal components of the crystal field; P_{θ_i} and P_{ϵ_i} are the momenta conjugate to Q_{θ_i} and Q_{ϵ_i}; μ_i is the effective mass of the ith phonon mode, and ω_i its angular frequency. V_i is the linear Jahn-Teller coupling coefficient between the doublet electronic state and the ith phonon mode; V_i is related to the Jahn-Teller stabilization energy, E_{JT_i}, through the relation

$$E_{\mathrm{JT}_i} = \frac{V_i^2}{2\mu_i\omega_i^2}. \tag{5}$$

τ, U_θ, and U_ϵ are the Hermitian electronic operators transforming as A_g and the θ, ϵ components of the two-dimensional irreducible representation E_g, in the S_6 point group. It is convenient to work in the complex electronic basis, writing the electronic wavefunctions in terms of their respective m_l and m_s quantum numbers as $|-1, \pm\frac{1}{2}\rangle$, $|1, \pm\frac{1}{2}\rangle$, with the quantization axis along the direction of the trigonal field. In this basis, U_θ and U_ϵ take the form of the Pauli matrices,

$$U_\theta = \begin{pmatrix} 0 & 1 \\ 1 & 0 \end{pmatrix}, \quad U_\epsilon = \begin{pmatrix} 0 & -i \\ i & 0 \end{pmatrix}. \tag{6}$$

In the presence of strain, the symmetry of the complex is lowered from S_6 to C_i and no symmetry blocking of the Hamiltonian is possible. Provided we confine our attention to linear Jahn-Teller coupling in the ${}^2E_g$ basis, strains of symmetry E_θ and E_ε have the same effect on the energies of the vibronic states. Therefore, for the purpose of our calculations, the two terms in the Hamiltonian representing the low symmetry crystal field, may be reduced to one, e_θ, where $2e_\theta$ is equivalent to the one-electron splitting of the ${}^2E_g$ ground term. All the matrix elements are then real,[6] which greatly simplifies the numerical calculation. If the electronic basis is extended to include the higher lying ${}^2A_g$ trigonal

term, then strains of five different symmetries act between the states in the larger basis and each strain has a different effect on the vibronic energy levels.[5] At sufficiently large trigonal fields, the error in neglecting coupling to the ^2A_g trigonal term is small, and we have been able to reproduce the g values of Dubicki and Riley for the same magnitude of $2e_\theta$ [Table III and parameter $\Delta(Eu)$ in their paper].[5]

The eigenvalues of the Hamiltonian (1) are determined by expanding the electronic basis in terms of the eigenstates of the two-dimensional harmonic oscillator, expressing the operators in the second quantization notation, evaluating the matrix elements, and bringing the vibronic matrix to diagonal form using a Lancoz algorithm. A listing of the matrix elements and details of the calculation, in the absence of low symmetry strain, have been presented previously.[6]

B. Approximate treatment for very weak Jahn-Teller coupling

By treating the strain and Zeeman interactions as consecutive perturbations to the crystal field wave functions, we obtain the following approximate expressions for the energy separation of the two Kramers doublets, and the ground state g values,

$$\Delta E \approx \lambda + \frac{2e_\theta^2}{\lambda}, \tag{7}$$

$$g_\parallel \approx 2\left(1-k\left(\frac{2\lambda^2}{\lambda^2+e_\theta^2}-1\right)\right), \quad g_\perp \approx -\frac{4e_\theta\lambda}{\lambda^2+e_\theta^2}. \tag{8}$$

When $e_\theta=0$, a finite first-order Zeeman splitting is obtained only when the magnetic field is directed out of the **xy** plane of the molecule, and then only by a partial quenching of orbital angular momentum. In the presence of strain, the orbital reduction factor, k, is accompanied by a term that decreases from unity with increasing e_θ. Strain also gives rise to a finite $g_\perp$, but only the spin part of the Zeeman interaction yields nonzero matrix elements, in contrast to $g_\parallel$. Note that the magnitude of $g_\perp$ and $g_\parallel$ increase to first-order and second-order in e_θ, respectively.

Although the symmetry of the complex is lowered from S_6 to C_i, the g-tensor remains axially symmetric. The degeneracy of g_x and g_y is accidental and is apparent only when the basis set is confined to the ^2E_g-ground term. Extending the electronic basis to include the higher lying ^2A_g trigonal term does lift the degeneracy of g_x and g_y but this splitting is shown to be very small for the magnitude of the trigonal field present.[5] This system has certain similarities to platinum doped into silicon, occupying a negatively charged vacancy, which has recently been treated in considerable detail.[20] As λ is reduced, the two Kramers doublets are more readily mixed by the low symmetry distortion, resulting in a steeper increase in the ground state g values with increasing e_θ. However, the magnitude of $g_\perp$, for a given value of $g_\parallel$, is not sensitive to the value of λ.

In order to examine the influence of weak Jahn-Teller coupling on the ground state g values, we construct analytical expressions for $g_\parallel$ and $g_\perp$, in the limit where $\hbar\omega+\lambda > \sqrt{2E_{JT}\hbar\omega} > e_\theta > B\beta$, restricting the basis set to the ground and first excited states of the harmonic oscillator. The wave functions are specified as, $|m_l, m_s, N, M\rangle$, where N and M are the principal quantum numbers of the 2D harmonic oscillator. No assumptions are made as to the relative magnitudes of $\hbar\omega$ and λ; in this instance, the new wavefunctions and energies of the states, which interact through an energy separation of $\hbar\omega+\lambda$, may be evaluated using perturbation theory, but the interaction between the states separated by $\hbar\omega-\lambda$ must be evaluated exactly. After treating the Jahn-Teller and strain interactions as consecutive perturbations to the crystal field wave functions, the new ground state wave functions are

$$\psi_{2\Gamma_6} = N\begin{pmatrix} |\pm 1,\mp\tfrac{1}{2},0,0\rangle - a|\mp 1,\mp\tfrac{1}{2},1,\pm 1\rangle \\ -e_\theta N_1^2\left(\frac{1}{\Delta_1}+\frac{b^2}{\Delta_2}\right)|\mp 1,\mp\tfrac{1}{2},0,0\rangle + e_\theta N_1^2\left(\frac{b}{\Delta_1}-\frac{b}{\Delta_2}\right)|\pm 1,\mp\tfrac{1}{2},1,\mp 1\rangle \\ +\frac{ae_\theta}{\hbar\omega-E_1}|\pm 1,\mp\tfrac{1}{2},1,\pm 1\rangle \end{pmatrix}, \tag{9}$$

where

$$a=\frac{\sqrt{2E_{JT}\hbar\omega}}{\hbar\omega+\lambda},$$

$$b=\frac{2\sqrt{2}\sqrt{E_{JT}\hbar\omega}}{\hbar\omega-\lambda+\sqrt{8E_{JT}\hbar\omega+\hbar\omega^2-2\hbar\omega\lambda+\lambda^2}},$$

$$N_1^2=\frac{1}{1+b^2}, \quad \Delta_1=E_2-E_1, \quad \Delta_2=E_3-E_1,$$

$$E_1=-\frac{2E_{JT}\hbar\omega}{\hbar\omega+\lambda},$$

$$E_2=\tfrac{1}{2}(\hbar\omega+\lambda-\sqrt{8E_{JT}\hbar\omega+\hbar\omega^2-2\hbar\omega\lambda+\lambda^2}), \text{ and}$$

$$E_3=\tfrac{1}{2}(\hbar\omega+\lambda+\sqrt{8E_{JT}\hbar\omega+\hbar\omega^2-2\hbar\omega\lambda+\lambda^2}).$$

$g_\parallel$ and $g_\perp$ are then given by

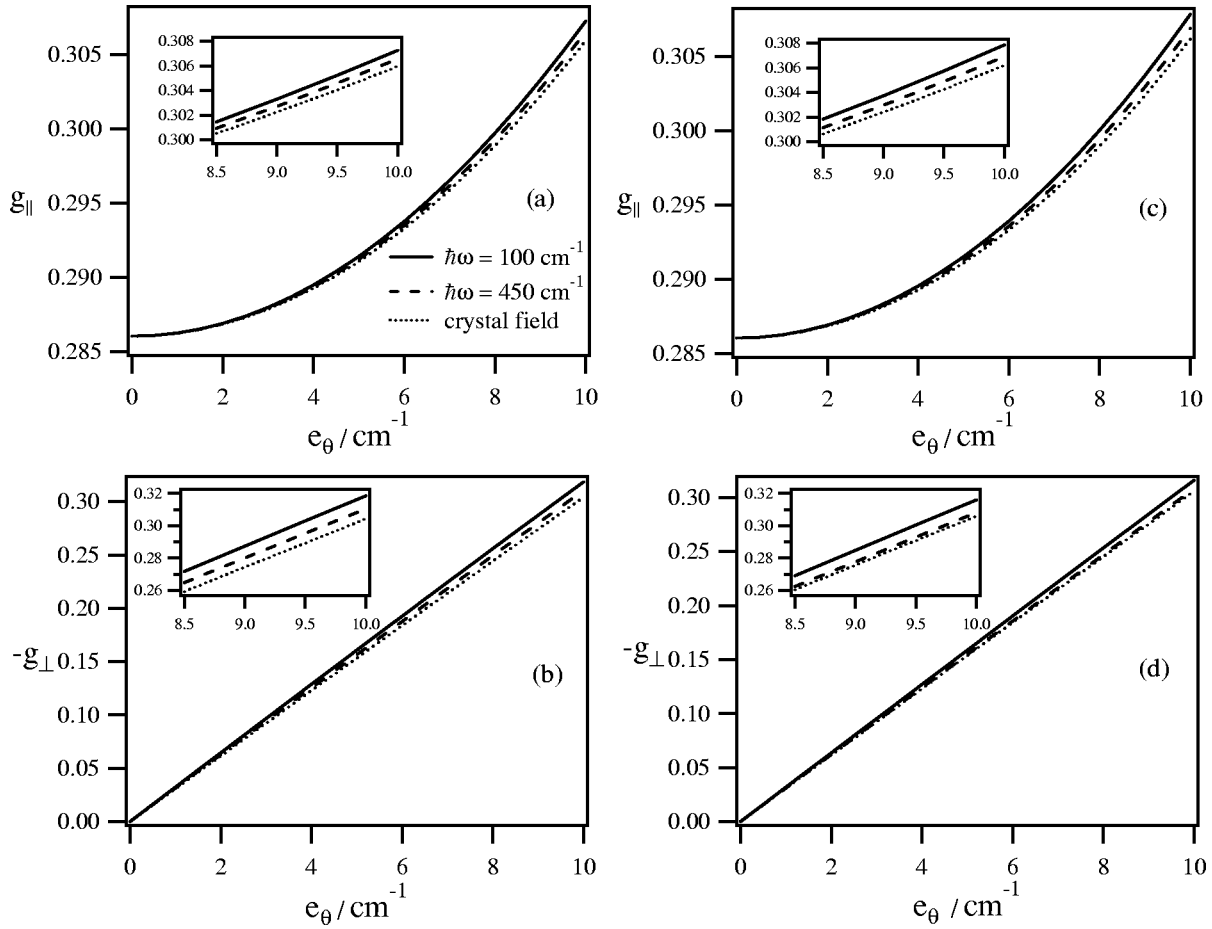

FIG. 1. Plots of $g_\parallel$ and $g_\perp$ vs e_θ, for different values of E_{JT} and $\hbar\omega$. Plots (a) and (b) were calculated by numerical diagonalization of the full vibronic Hamiltonian; plots (c) and (d) were calculated from Eqs. (11) and (13), respectively. In each case, the parameters were chosen to yield a value of $g_\parallel = 0.286$ at $e_\theta = 0$. For all the crystal field plots (solid line) $E_{\mathrm{JT}} = 0$, $\lambda = 130\ \mathrm{cm}^{-1}$, and $k = 0.857$. For the Jahn-Teller plots $k = 0.88$, $\lambda = 130\ \mathrm{cm}^{-1}$, and E_{JT} and $\hbar\omega$ varied to give $g_\parallel = 0.286$ at $e_\theta = 0$. The plots for which $\hbar\omega = 450\ \mathrm{cm}^{-1}$ (dotted line) were calculated with $E_{\mathrm{JT}} = 5\ \mathrm{cm}^{-1}$ [(a) and (b)] and $E_{\mathrm{JT}} = 4.95\ \mathrm{cm}^{-1}$ [(c) and (d)]; the plots for which $\hbar\omega = 100\ \mathrm{cm}^{-1}$ (broken line) were calculated with $E_{\mathrm{JT}} = 3.49\ \mathrm{cm}^{-1}$ [(a) and (b)] and $E_{\mathrm{JT}} = 3.50\ \mathrm{cm}^{-1}$ [(c) and (d)].

$$g_\parallel = 2N^2\left(\begin{array}{c} 1-k+a^2(k+1)+\left(e_\theta N_1^2\left(\dfrac{1}{\Delta_1}+\dfrac{b^2}{\Delta_2}\right)\right)^2(k+1) \\ +\left(e_\theta N_1^2\left(\dfrac{b}{\Delta_1}-\dfrac{b}{\Delta_2}\right)\right)^2(-k+1)+\left(\dfrac{a e_\theta}{\hbar\omega - E_1}\right)^2(-k+1) \end{array}\right) \tag{10}$$

$$\approx 2\left(1-k\left(\frac{2\lambda^2}{\lambda^2+e_\theta^2}-1\right)\left(\frac{(\hbar\omega+\lambda)^2-2E_{\mathrm{JT}}\hbar\omega\left(1+\dfrac{2e_\theta^2}{\lambda^2}\right)}{(\hbar\omega+\lambda)^2+2E_{\mathrm{JT}}\hbar\omega\left(1+\dfrac{2e_\theta^2}{\lambda^2}+\dfrac{2e_\theta^2}{\hbar\omega^2}+\dfrac{4e_\theta^2}{\hbar\omega\lambda}\right)}\right)\right), \tag{11}$$

$$g_\perp = -4e_\theta N^2\left(N_1^2\left(\frac{1}{\Delta_1}+\frac{b^2}{\Delta_2}\right)+\frac{a^2}{\hbar\omega - E_1}\right) \tag{12}$$

$$\approx -\frac{4e_\theta\lambda}{\lambda^2+e_\theta^2}\left(1+\frac{4E_{\mathrm{JT}}\lambda}{(\hbar\omega+\lambda)^2+2E_{\mathrm{JT}}(2\hbar\omega+\lambda)}\right). \tag{13}$$

The new expressions for $g_\parallel$ and $g_\perp$, set out in Eqs. (11) and (13), are analogous to the crystal field expressions (7) and (8) except that they are each multiplied by an extra term which tends to 1 as $E_{\mathrm{JT}} \to 0$. These terms reflect the effective quenching of k and λ as viewed by the ground state.[21] In Fig. 1 are presented calculations of $g_\parallel$ and $g_\perp$, as a function of e_θ, for small values of E_{JT}. Plots (c) and (d) were calculated using Eqs. (11) and (13), respectively, for different values of $\hbar\omega$, and these compare well with plots (a) and (b), which were calculated by numerical diagonalisation of the full vibronic Hamiltonian. Although quantitative agreement becomes poorer with increasing E_{JT}, we find that the general dependence and inter-relation of $g_\parallel$ and $g_\perp$ on the parameters

of the vibronic Hamiltonian, are still described by Eqs. (11) and (13). The crystal field plots ($E_{JT}=0$) were calculated with $k=0.857$, to give $g_{\|}=0.286$ at $e_{\theta}=0$. The plots which include Jahn-Teller coupling were calculated with $k=0.88$; in each case the value of E_{JT} was adjusted to give $g_{\|}=0.286$ at $e_{\theta}=0$.

In the absence of strain, the reduction factor, which accompanies k, decreases with increasing E_{JT} (giving rise to a larger value of $g_{\|}$) but has a complicated dependence on $\hbar\omega$; for high and moderate values of $\hbar\omega$, the reduction factor decreases with decreasing $\hbar\omega$, but at low values of $\hbar\omega$, increases with decreasing $\hbar\omega$ (see also Table I Ref. 6).

As $\hbar\omega$ decreases and E_{JT} increases, the first excited state approaches the ground state, and the two states can more effectively couple through a low symmetry perturbation. This equates to an effective quenching of the spin–orbit interaction. In order to maintain $g_{\|}$ constant at $0.286(e_{\theta}=0)$, upon decreasing $\hbar\omega$ from 450 to 100 cm^{-1}, E_{JT} is decreased slightly, as described in the Fig. 1 caption. The net effect of the change in E_{JT} and $\hbar\omega$ is to give rise to a more rapid increase in the ground state g values with increasing e_{θ}, as seen from Fig. 1. In other words, coupling to a low energy phonon facilitates the quenching of λ. From inspection of Eqs. (11) and (13), it is noted that the vibronic factors, which accompany the crystal field expressions for the ground state g values, have rather different forms; and it is found that decreasing the phonon energy also gives rise to a larger value of $g_{\perp}$, for a given value of $g_{\|}$. This is apparent from calculations using Eqs. (11) and (13) but is shown most transparently in Fig. 2(c), which is discussed in detail in Secs. IV and V. This result holds true over a wide parameter range, and is important, as the dependence of the $g_{\|}$ vs $g_{\perp}$ relation on $\hbar\omega$ facilitates the determination of this parameter.

C. Calculation of EPR simulations

The principal ground state g values, $g_{\|}$ and $g_{\perp}$, were calculated numerically by diagonalizing the Hamiltonian matrix once with $B_z=6000\,G$, $B_x=B_y=0$; and once with $B_x=6000\,G$, $B_z=B_y=0$. With θ defined as the angle between the static magnetic field and the principal direction of the g matrix, g_{θ} is given by

$$g_{\theta}^2=g_{\|}^2\cos^2\theta+g_{\perp}^2\sin^2\theta, \tag{14}$$

providing the applied magnetic field is small enough so that the pronounced third-order Zeeman term is negligible.[11]

EPR simulations are presented and discussed in Sec. V. The spectra were calculated in two steps. First, a library of g values was calculated for various values of e_{θ}, all other parameters being held constant. A total of 4001 pairs of principal g values were calculated for values of e_{θ} between 0 and 22 cm^{-1}, in equidistant steps; g_{θ} was calculated according to Eq. (14), and the resonant magnetic fields, in Gauss, according to

$$B_{res(e_{\theta},\theta)}=\frac{h\nu}{\beta g(\theta)}, \tag{15}$$

where $\nu=9.5\,GHz$.

Second, EPR spectra were calculated as a superposition of resonances arising from each of the 4001 chemically distinct species. Each EPR resonance was assigned a first derivative Gaussian band shape. The intensity of the EPR line at field B for the ith value of e_{θ}, $I(B)_i$, was calculated according to

$$I(B)_i=\frac{-2\ln 2(B-B_{res})\exp\left(\frac{-\ln 2(B-B_{res})^2}{\gamma(\theta)^2}\right)p}{\gamma(\theta)^2}; \tag{16}$$

$\gamma(\theta)$ defines the linewidth and is given by

$$\gamma(\theta)=\frac{\sigma}{g_{\theta}}, \tag{17}$$

where σ is the full width at half height; p is the transition probability, given by

$$p=\frac{g_{\perp}g_{\|}}{g_{\theta}^2}. \tag{18}$$

The total intensity at field B, $I(B)_{total}$ was then calculated according to

$$I(B)_{total}=\sum_{i=1}^{i=4001} I(B)_i w(B)_i, \tag{19}$$

The contribution of each complex to the heterogeneously broadened EPR spectrum was weighted according to a Gaussian distribution [Fig. 7(a)]

$$w(B)_i=\exp\left(\frac{-\ln 2(e_{\theta_i}-e_{\theta_m})^2}{e_{\theta_w}^2}\right), \tag{20}$$

where e_{θ_i} is the strain parameter pertaining to the ith complex, e_{θ_m}, the mean strain value, about which the strain-broadened band is centered, and e_{θ_w} the width at half height of the strain distribution. The weighting scheme used to calculate the simulations presented in Fig. 7(b), employs a sum of two such Gaussian functions.

IV. RESULTS

CW EPR spectra of Cs[Al:Ti]SH (2% titanium(III)) with the applied field along a [111] axis are presented in Fig. 2(a). The spectra were recorded on the same sample at different times. The relaxation times are strongly temperature dependent, and the spectrum could be observed only at temperatures below the lambda-point of liquid helium, as reported previously.[1,4,6] All the spectra were recorded with a microwave power of 0.01 mW; at powers greater than this, saturation effects are evident, with the low field lines saturating first. There are slight differences in the three spectra recorded at the X-band. It is likely that this is due to partial, and variable saturation, due to small variations in the temperature at the sample, between the three runs. The spectrum consists of at least seven lines which supports the assignment to transitions from chemically distinct species of titanium(III),[1,5] as opposed to transitions within low lying vibronic levels of a single titanium(III) ion, as the latter model can account for only three lines.[4] The spectrum at S-band is also presented in

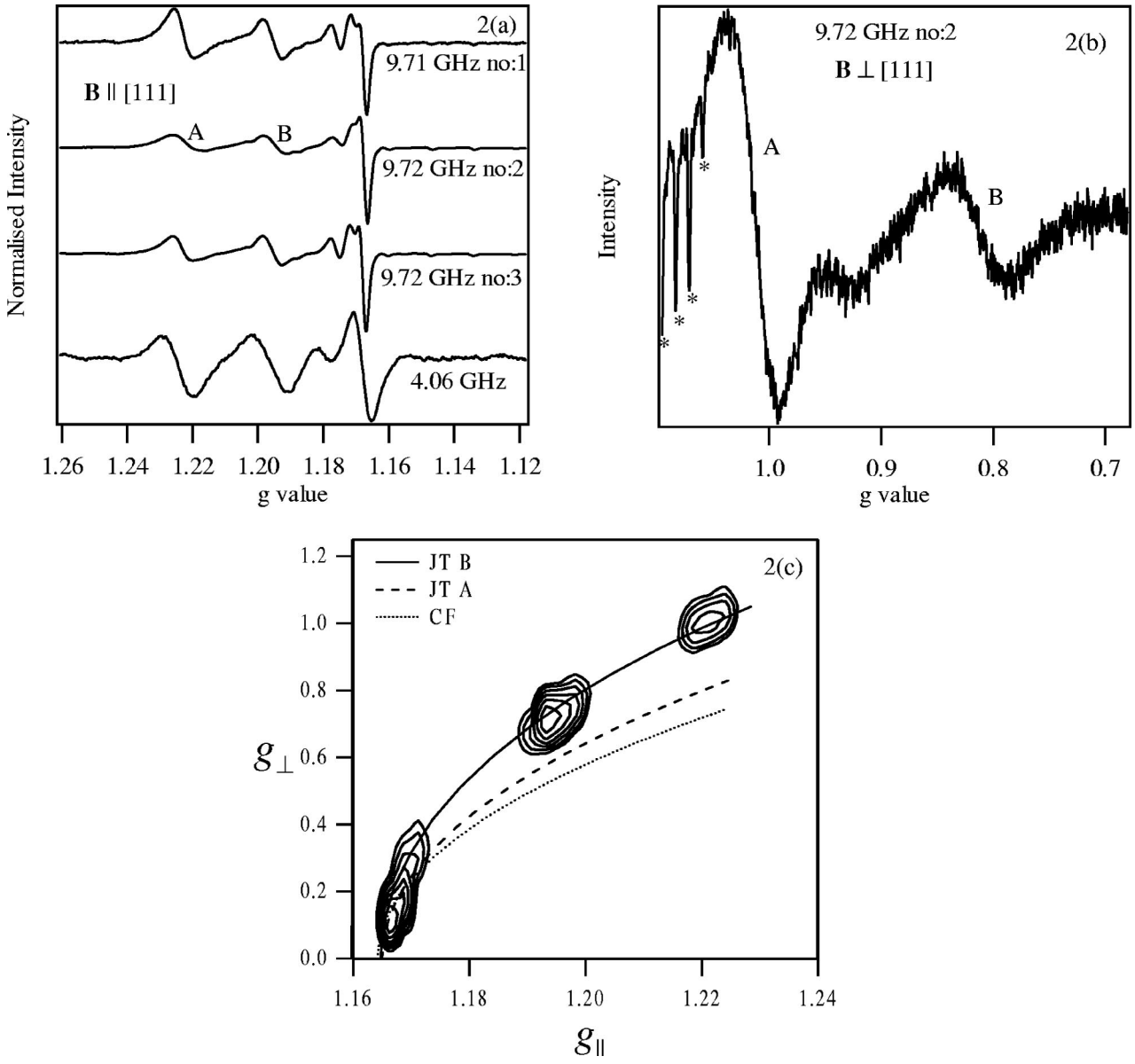

FIG. 2. CW- and pulsed-EPR spectra of Cs[Al:Ti]SH (2% titanium(III)). All spectra were obtained in conjunction with a Bruker dielectric resonator. The temperature of the cavity was ≈1.7 K for all the spectra; the exact temperature at the sample was not determined, however. The CW spectra presented in (a) and (b) were each recorded with a modulation amplitude of 4 G, a resolution of 2048 points, a microwave power of 0.01 mW, and an excitation frequency of ≈9.7 GHz. The field positions of the two, prominent low field resonances can be followed for all crystal orientations and are labeled A and B in spectrum No. 2. Note that the field axis spans 800 G in (a) and 3850 G in (b). Transitions marked ∗ in (b) are assigned to Ti hyperfine lines arising from a set of titanium(III) complexes, whose z axes coincide with a [111] direction of the crystal differing to that of the titanium(III) complexes, which give rise to resonances A or B. (c) Shows the field swept nutation spectra transformed to give a two-dimensional plot of $g_\parallel$ against $g_\perp$. The $g_\perp$ axis was scaled to the value of the low field line (resonance A), obtained from the CW measurements [$g_\parallel = 1.220(3)$, $g_\perp = 1.012(4)$]. The parameters used in the pulsed sequence were $\tau = 200$ ns, $T = 1000$ ns, $dt = 8$ ns with a resolution of 100 points. The time domain spectrum was processed by applying a linear baseline correction and a Gaussian window function before zero filling to 256 points and Fourier transforming. In the field axis, 32 field steps of 12 G were made across the spectrum. Overlaid on the contour plot are three theoretical curves of $g_\parallel$ vs $g_\perp$, calculated as a function of strain for different ligand field and vibronic coupling parameters. The parameters used were as follows: CF, was calculated using a purely crystal field model ($E_{JT} = 0$) with $\lambda = 130\ \mathrm{cm}^{-1}$ and $k = 0.418$; JT A, was calculated with $\lambda = 130\ \mathrm{cm}^{-1}$, $k = 0.88$, $\hbar\omega = 450\ \mathrm{cm}^{-1}$, $E_{JT} = 176.5\ \mathrm{cm}^{-1}$; JT B, was calculated with $\lambda = 130\ \mathrm{cm}^{-1}$, $k = 0.88$, $\hbar\omega_1 = 53\ \mathrm{cm}^{-1}$, $E_{JT1} = 53 \times 1.0525$, $\hbar\omega_2 = 894\ \mathrm{cm}^{-1}$, $E_{JT2} = 90.1 \times 1.0525\ \mathrm{cm}^{-1}$.

Fig. 2(a), and is seen to be analogous to the *X*-band spectrum. If the EPR lines were to originate from transitions between levels of a pseudo $S = 3/2$ spin system subject to a small zero-field splitting, as postulated by Shing and Walsh,[4] the spectrum would be expected to be strongly dependent on the frequency of the B_1 field. Therefore, the measurements at the *S*-band confirm assignment of the multiline EPR spectrum to chemically distinct titanium(III) species.

The $g_\parallel$ values, T_1 relaxation times (determined using the inversion-recovery technique) and calculated homogeneous linewidths σ_{hom}, for the prominent EPR lines, are as follows: $g_\parallel = 1.220(3)$, $T_1 = 2.78\ \mu$s, $\sigma_{hom} = 0.21$ G; $g_\parallel = 1.195(3)$, $T_1 = 2.19\ \mu$s, $\sigma_{hom} = 0.27$ G; $g_\parallel = 1.172(3)$, $T_1 = 0.61\ \mu$s, $\sigma_{hom} = 1$ G; $g_\parallel = 1.168(3)$, $T_1 = 0.69\ \mu$s, $\sigma_{hom} = 0.89$ G. There is some uncertainty in the values obtained from the fitting procedure, and from some variations in the

experimental parameters. However, it is certain that the relaxation times are no shorter than these values, though they may be longer. The decrease in the relaxation times across the spectrum are consistent with the power saturation measurements. The calculated homogeneous linewidths are much smaller than the overall linewidths, and hence, homogeneous broadening has only a small contribution to the linewidths at this temperature; the dominant contribution must be inhomogeneous broadening. The low-field EPR lines broaden considerably on rotating the crystal in the {110} plane and well-resolved spectra can be obtained only within ≈35° of the [111] axis. Nevertheless, the field positions of the two, prominent, low field resonances can be followed for all orientations of the crystal, and the principal g values are determined as $g_{\|}=1.220(3)$, $g_{\perp}=1.012(4)$ [resonance A in Figs. 2(a) and 2(b)] and $g_{\|}=1.195(3)$, $g_{\perp}=0.815(9)$ (resonance B). The respective linewidths of these resonances, as defined by the peak to peak distance, increase from ≈45 and ≈40 G (*X*-band) with the [111] axis parallel to the applied field, to ≈300 and ≈700 G with the [111] axis perpendicular to the applied field [Fig. 2(b)]. The relaxation times decrease sharply with increasing θ. For example, the value of T_1 for the line for which $g_{\|}=1.220(3)$, falls from 2.78 to 0.29 μs as θ increases from 0 to 10°. The sharp decrease in T_1 with increasing θ is in accordance with the theory of Dubicki and Riley,[5] but cannot alone explain the pronounced increase in the linewidths.

The transition for which $g_{\|}=1.168(3)$ shows well-resolved titanium hyperfine structure with $A_{\|}=37.6(5)\times10^{-4}\,\mathrm{cm}^{-1}$ for both isotopes. The linewidth of this transition is not strongly dependent on the crystal orientation but its position can be monitored only within ≈55° of the [111] axis. Beyond this angle, its position is beyond the magnetic field range of the spectrometer. The value of $g_{\perp}$ using CW EPR can be determined only by extrapolation and is found to be ~0. We note that $g_{\perp}$ cannot be exactly zero as the nutation frequency, and hence the transition probability would also be zero. The values of $g_{\perp}$ for the other transitions identified in Figs. 2(a) and 2(b) cannot be determined with reasonable precision by CW EPR; therefore CW EPR does not afford the precise determination of the principal g values.

In order to characterize the spectrum further, a 2D field-swept nutation experiment was performed, with the applied magnetic field parallel to the [111] direction of the crystal. The magnetic field axis can be transformed into $g_{\|}$, and the distribution of nutation frequencies converted to values of $g_{\perp}$ by calibration against the transition for which $g_{\|}=1.220(3)$ and $g_{\perp}=1.012(4)$. The resultant spectrum therefore has axes of $g_{\|}$ and $g_{\perp}$ and is displayed in Fig. 2(c). The advantage of the nutation method is seen in the extra information contained in the 2D spectrum. The CW spectra yield a pair of $g_{\|}$ and $g_{\perp}$ values for each transition. In the 2D spectrum, however, a continuous spectrum in two dimensions is produced with $g_{\|}$ and $g_{\perp}$ for each point. The spectrum highlights the inter-relation between $g_{\|}$ and $g_{\perp}$, which is seen across the whole spectrum. It is seen from Fig. 2(c) that $g_{\perp}$ varies across each of the lines seen in the EPR spectrum, which suggests that the width of these lines results from inhomogeneous broadening. It is evident, therefore, the spectrum originates from a distribution of sites with a range of g values. If relaxation broadening were the dominant contribution to the linewidth, we would expect each peak in the 2D nutation spectrum to have a constant nutation frequency, i.e., the ridge of the peaks would be parallel with the field axis; this is obviously not consistent with the experimental spectrum. The precision with which the 2D-nutation spectrum reproduces the g value distribution will be affected by several experimental factors. Some of these will lead to a broadening of the spectrum in both $g_{\|}$ and $g_{\perp}$, which will smooth the spectrum resulting in a loss of detail. It could be argued that the distribution seen arises primarily as a consequence of experimental broadening; however, the contour profiles are highly asymmetric, which is not consistent with this interpretation. In addition, $g_{\perp}$ values below 0.1 will not be accurately reproduced with the parameters used in the experiment. Therefore, it is likely that the distribution extends to lower $g_{\perp}$ than is indicated by the 2D-nutation spectrum. To record accurately this part of the spectrum, it would be necessary to use either a larger B_1 field, which is limited by the spectrometer, or to use a longer T in the experiment, which is limited by the relaxation times of the system.

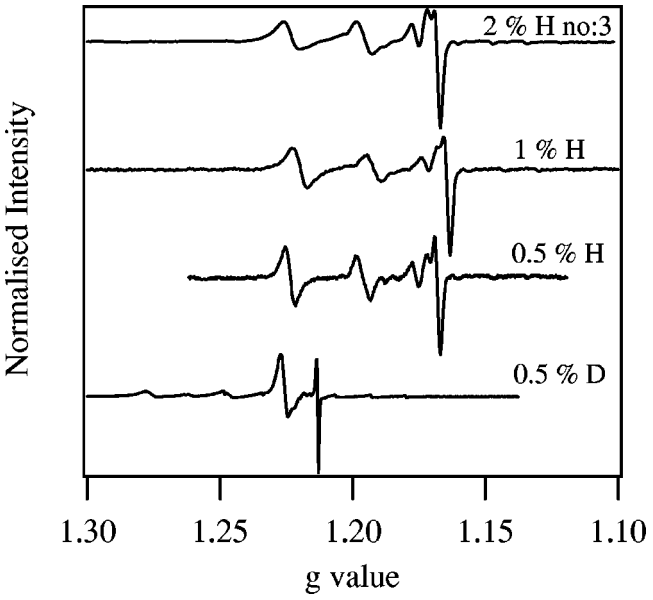

FIG. 3. *X*-band EPR spectra of Cs[Al:Ti]SH as a function of titanium(III) concentration. All spectra recorded with the [111] direction of the crystal aligned with the external magnetic field, at ≈1.7 K. The Cs[Al:Ti]SH spectra were recorded with a microwave power of 0.01 mW and a modulation amplitude of 4 G. The spectra of the 2% and 0.5% samples were obtained using a Bruker dielectric resonator, and the spectrum of the 1% sample was obtained using a Bruker ER 4122 SHQ resonator. The EPR spectrum of Cs[Al:Ti]SD was obtained using a Bruker dielectric resonator employing a microwave power of 0.01 Mw and a modulation amplitude of 2 G.

In Fig. 3 are presented spectra of Cs[Al:Ti]SH with approximate titanium(III) starting concentration of 2%, 1%, and 0.5%, along with the EPR spectrum of the deuterated analog [0.5% titanium(III)]. The samples were prepared, and the EPR spectra recorded, under the same conditions; the exact concentration of titanium(III) in the crystals has not been determined, however. All the spectra presented in Fig. 3 were recorded with the [111] direction of the crystal aligned with the external magnetic field. The spectra of the

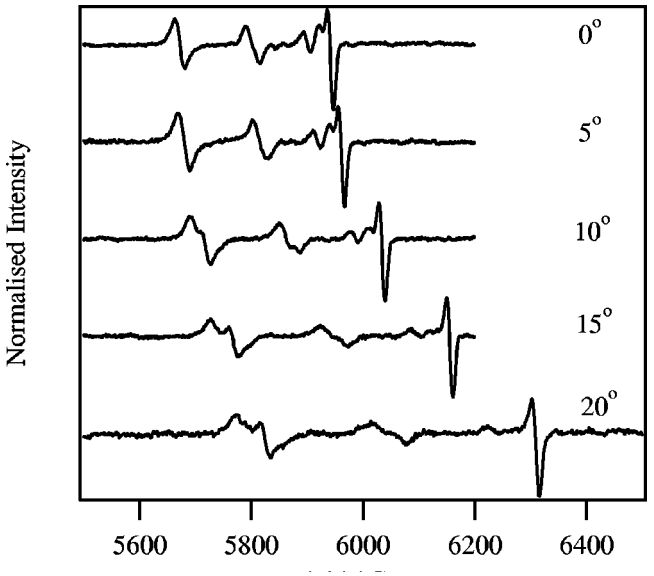

FIG. 4. Angular dependence of the CW-EPR spectra of Cs[Al:Ti]SH (0.5% titanium(III)). The spectra were obtained with a modulation amplitude of 4 G, a resolution of 2048 points, and an excitation frequency of 9.72 GHz, at ≈1.7 K. The magnetic field was in a {110} plane and the angles that the direction of B makes with the [111] direction of the crystal are indicated on the figure.

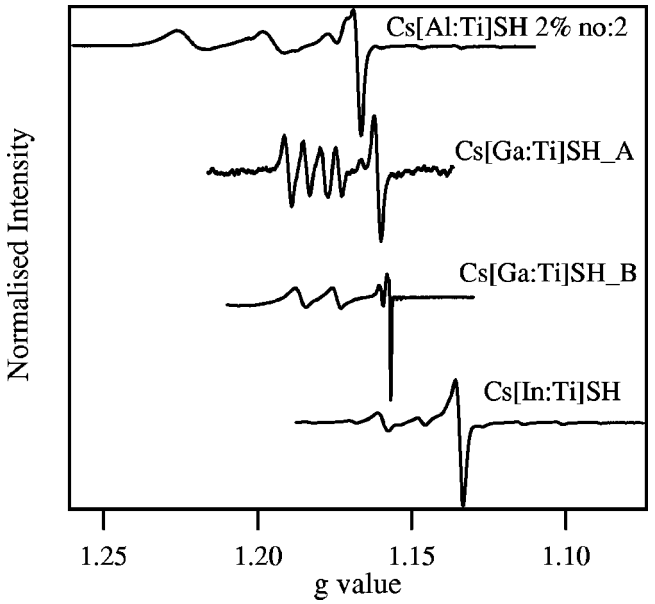

FIG. 5. EPR spectra of Cs[Al:Ti]SH (2% titanium(III)), Cs[Ga:Ti]SH_A (0.5% titanium(III)); Cs[Ga:Ti]SH_B (1% titanium(III)) and Cs[In:Ti]SH (1% titanium(III)). Samples Cs[Ga:Ti]SH_A and Cs[Ga:Ti]SH_B were prepared by different methods, as described in the text. All spectra were obtained at ≈1.7 K with the [111] direction of the crystal aligned with the external magnetic field. Spectra of Cs[Al:Ti]SH, Cs[Ga:Ti]SH_A, and Cs[In:Ti]SH were obtained at the *X*-band (≈9.7 GHz), whereas the spectrum of Cs[Ga:Ti]SH_B was obtained at the *W*-band (95.0603 GHz).

Cs[Al:Ti]SH samples are very similar. There is no significant change in the relative intensities or the linewidths of the EPR lines in this titanium(III) concentration range. The EPR spectrum of Cs[Al:Ti]SD is markedly different from the hydrated samples. The linewidth of the high field line is much narrower in the deuteriated sample, whereas there is little change in the linewidths of the lower field resonances. This suggests that inhomogeneous broadening due to the superhyperfine interaction largely determines the linewidth of the narrow high field resonance but not the broader lower field resonances. The EPR spectrum of an ^{18}O enriched (≈90%) sample has also been obtained and presented previously,[6] and was found to have the same general appearance as the spectrum of Cs[Al:Ti]SH, prepared using water of natural isotopic abundance.

The angular dependence of the EPR spectrum of Cs[Al:Ti]SH [0.5% titanium(III)] is shown in Fig. 4. Upon rotation in the {110} plane the EPR lines broaden considerably, as observed for Cs[Al:Ti]SH (2% titanium(III)). However, the spectra of Cs[Al:Ti]SH (0.5% titanium(III)) are better resolved, with the two low field lines seen to split into at least two components on increasing θ. The EPR spectra of Cs[Al:Ti]SD, Cs[Ga:Ti]SH, and Cs[In:Ti]SH exhibit similar behavior. Clearly, in order to provide a comprehensive description of this system, an adequate account of these curious spectra must be provided.

In Fig. 5 are shown EPR spectra of Cs[Al:Ti]SH, Cs[Ga:Ti]SH, and Cs[In:Ti]SH; all the spectra were obtained with the [111] direction of the crystal aligned close to the direction of the external magnetic field. Crystals Cs[Ga:Ti]SH_A and Cs[Ga:Ti]SH_B were prepared by methods employing fast and slow deposition of material, respectively, as described in Sec. II A. The spectra were recorded using an excitation frequency of ≈9.7 GHz, except the spectrum obtained from Cs[Ga:Ti]SH_B, where an excitation frequency of 95.0603 GHz was employed. All spectra consist of a number of resonances, with differing linewidths. For the spectra collected at the *X*-band, the value of $g_\perp$ for the high-field line was determined to be ~0 from the angular dependence of the CW spectra; it was not possible to monitor the angular dependence of the *W*-band EPR spectra of Cs[Ga:Ti]SH_B. The value of $g_\parallel$ for the high-field line is seen to decrease as the ionic radius of the host tervalent cation increases. This can result either from a larger value of k, or a smaller value of E_{JT}. The resonances observed in the spectrum of Cs[Al:Ti]SH_A span a larger range in $g_\parallel$ compared to the spectra of Cs[Ga:Ti]SH or Cs[In:Ti]SH. This has important implications for the magnitude of strain, which the titanium(III) cations are subject to within the crystal, as we shall discuss in the next section. Figure 5 contains EPR spectra of Cs[Ga:Ti]SH obtained from two different samples, at two different frequencies. The high-field line found in the spectrum obtained for Cs[Ga:Ti]SH_A appears to occur at a slightly higher g value compared to its counterpart in the spectrum of Cs[Ga:Ti]SH_B. However, the g values for the two lines are the same, allowing for the uncertainty in the field calibration, and crystal alignment. Allowing for this offset, the lowest field resonance observed is found at the same g value for the two samples. Furthermore, for almost every resonance observed in the spectrum of Cs[Ga:Ti]SH_A, there is a corresponding resonance at more or less the same g value found in the spectrum of Cs[Ga:Ti]SH_B. However, the two spectra do differ very significantly in terms of the relative intensities and linewidths. This suggests that the form of the EPR spectrum obtained depends on the way the

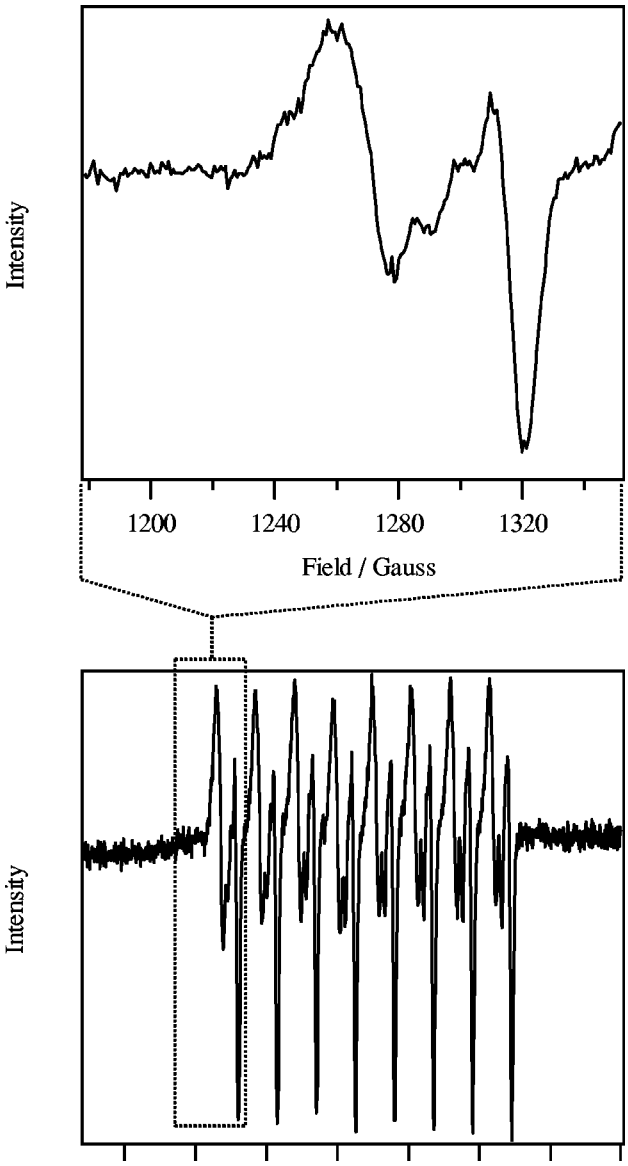

FIG. 6. EPR spectrum of Cs[Al:V]SH (≈1% vanadium(III) in solution). The spectrum was obtained at ≈5 K using a dual-mode resonator (ER 4116 DM) operating in parallel mode. A microwave power of 25 mW, and a modulation amplitude of 4 G, was employed for the data collection. The [111] direction of the crystal was aligned parallel with the static field.

crystal is prepared. Indeed, the spectra of Cs[Al:Ti]SH, presented in this paper, are notably different from the spectra published by Woonton and MacKinnon,[1] and by Shing and Walsh[4] (when in both cases no details on sample preparation were given). The linewidths of the low field structure in the sample Cs[Ga:Ti]SH_B, are much greater compared to Cs[Ga:Ti]SH_A, when measured in the field domain, which again, is consistent with the interpretation that the origin of the large linewidths of some of the EPR lines is inhomogeneous broadening.

In Fig. 6 is shown the EPR spectrum of Cs[Al:V]SH, collected with the [111] direction of the crystal, and the magnetic vector of the B_1 field, aligned parallel to the external magnetic field. We include this spectrum, as it is a sensitive measure of low symmetry perturbations of the vanadium(III) hexa-aqua cation, in a manner analogous to the EPR spectrum of Cs[Al:Ti]SH. The $^3A_g(S_6)$ ground term is split by the combined effects of spin–orbit coupling and the trigonal field into a singlet and higher lying doublet.[22,23] With the oscillating magnetic field component of the microwaves applied parallel to the external magnetic field, the selection rule, $\Delta m_s = 0$ applies. The $\Delta m_s = 2$ transition, shown in Fig. 6, is therefore forbidden in trigonal symmetry but becomes allowed in lower symmetry, as this has the effect of mixing the $m_s = 1$ and $m_s = -1$ states, removing the degeneracy. Thus, by analogy with the EPR spectrum of Cs[Al:Ti]SH, a low symmetry crystal field provides intensity for the EPR transition, and shifts the resonance to lower field. Due to the hyperfine interaction, an eight line spectrum is expected to result from each chemically distinct vanadium(III) species. Eight sets of at least four line are observed, as shown in Fig. 6. This must be interpreted in terms of chemically distinct vanadium(III) species. The spectra of Cs[Al:Ti]SH and Cs[Al:V]SH each display a sharp high field line, arising from species where strain is minimal, and broader lower field resonances, corresponding to lower symmetry species. This demonstrates that the multiline EPR spectrum of Cs[Al:Ti]SH is a consequence of doping an impurity into CsAlSH, rather than any peculiar manifestation of the Jahn-Teller effect.

V. DISCUSSION

The variation in $g_\perp$ across the spectrum of Cs[Al:Ti]SH suggests a variation in the magnitude of the low symmetry distortion, as described by the parameter, e_θ. Superimposed on the experimental data in Fig. 2(c) are three theoretical plots, calculated with different sets of parameters. In each case the parameters were adjusted to reproduce the g values of the high field line where strain is minimal; $g_\parallel$ and $g_\perp$ were then calculated as a function of e_θ, all other parameters being kept constant.

The plot denoted CF was calculated using a purely crystal field model. With e_θ and $E_{JT} = 0$, $g_\parallel$ depends entirely upon k which was set to 0.418, to give $g_\parallel = 1.164$. The calculated $g_\parallel$ vs $g_\perp$ relation, as a function of e_θ, is shown to give a poor reproduction of the experimental data; $g_\parallel$ and $g_\perp$ are calculated to be 1.224 and 0.7428, respectively, for $e_\theta = 26\,\mathrm{cm}^{-1}$ and λ set to 130 cm^{-1}, this compares to $g_\parallel = 1.220(3)$ and $g_\perp = 1.012(4)$ determined for resonance A. As stated earlier, the value of $g_\perp$ for a given value of $g_\parallel$ is not dependent upon the value of λ.

Plots JTA and JTB were calculated by diagonalization of the full vibronic Hamiltonian. In both calculations, k was fixed at 0.88 and λ set to 130 cm^{-1}. For plot JTA, $\hbar\omega = 450\,\mathrm{cm}^{-1}$, the value assumed by Dubicki and Riley,[5] and $E_{JT} = 176.5\,\mathrm{cm}^{-1}$. Plot JTB employs a two mode model with $\hbar\omega_1 = 53$, $E_{JT1} = 1.0525 \times 53$ and $\hbar\omega_2 = 894$, $E_{JT2} = 1.0525 \times 90.1\,\mathrm{cm}^{-1}$, in keeping with the two-mode model used to fit the magnetic susceptibility.[6] Coupling to the low energy phonon dominates the magnetic properties of the ground state, and plot B can be reproduced using an effective frequency of $\hbar\omega \approx 100\,\mathrm{cm}^{-1}$. Compared to calculation CF, JTA does provide a better reproduction of the experimental data; however, for a given value of $g_\parallel$, the experimental value of $g_\perp$ is still significantly greater than predicted; for $e_\theta = 16\,\mathrm{cm}^{-1}$, $g_\parallel$ and $g_\perp$ are calculated to be 1.2252 and 0.8340, respectively. In

Sec. III, we discussed the sensitivity of the $g_{\|}$ vs $g_{\perp}$ relation to the parameters of the vibronic Hamiltonian. In general, coupling to a lower energy phonon gives rise to a greater value of $g_{\perp}$ for a given value of $g_{\|}$. This is clearly seen from Fig. 2(c). Plot B provides an excellent reproduction of the experimental data, as the fit passes through the center of each contour. For $e_{\theta}=11\,\mathrm{cm}^{-1}$, $g_{\|}$ and $g_{\perp}$ are calculated to be 1.220 and 0.989, respectively. These results are consistent with our previous analysis of the variation of the effective magnetic moment of CsTiSH, with temperature.[6] Compared to the parameters used to model the magnetic data of CsTiSH, we have increased the values of E_{JT} by 5.25% to fit the current data set.

If e_{θ} is increased a little further to $\approx 14\ \mathrm{cm}^{-1}$, we obtain $g_{\|}=1.25$, $g_{\perp}=1.16$. These numbers compare well to the experimental g values of CsTiSH (Ref. 24) ($g_{\|}=1.25, g_{\perp}=1.14$). Thus, based on these calculations, the one-electron splitting of the ground E_g orbital set, which results from the cooperative Jahn-Teller phase transition of CsTiSH, is estimated to be of the order of $28\ \mathrm{cm}^{-1}$. It should be mentioned that the g values of CsTiSH can also be reproduced with $\hbar\omega=450\,\mathrm{cm}^{-1}$, the one electron splitting set to $56\ \mathrm{cm}^{-1}$ and with k and λ reduced to 0.75 and $120\ \mathrm{cm}^{-1}$, respectively, as shown by Dubicki and Riley.[5] However, this lower value of k is not consistent with the asymptotic value of the susceptibility,[6] which depends upon k only. In addition, the calculated eigenvalues are not in agreement with the available Raman data.[25,26] Although $28\ \mathrm{cm}^{-1}$ is a fair estimate of the one-electron splitting, this quantity cannot be estimated precisely from our EPR data, as it is very sensitive to the parameters of the vibronic Hamiltonian. Furthermore, our calculations ignore higher order effects, which warp the potential energy surface, and so assist in localizing the titanium(III) complexes into distorted configurations.

The relative intensities of the EPR lines of Cs[Al:Ti]SH change very little as the titanium(III) concentration is decreased from 2% to 0.5% of the total tervalent cation concentration in solution. Furthermore, Woonton and MacKinnon[1] measured EPR spectra of crystals of Cs[Al:Ti]SH down to 0.05%, but do not report any change in the spectrum, resulting from the lower titanium(III) concentration.[1] This would suggest that the unusual spectrum does not result from any form of cooperative interaction of titanium(III) ions. Furthermore, evidence for chemically distinct vanadium(III) species is also found in the EPR spectrum of Cs[Al:V]SH. We suggest, therefore, that the anomalous EPR spectrum of Cs[Al:Ti]SH is simply due to a mismatch of the ionic radii of the dopant and host tervalent cations. This is reflected in the EPR spectra shown in Fig. 5. The resonances observed for Cs[Al:Ti]SH are spread over a wider range in g value, compared to Cs[Ga:Ti]SH and Cs[In:Ti]SH. This implies that the titanium(III) complexes, giving rise to the low field resonances in the spectrum of Cs[Al:Ti]SH, are subject to a larger deviation from trigonal symmetry compared to their counterparts in Cs[Ga:Ti]SH and Cs[In:Ti]SH. We have recently obtained high-field multifrequency EPR data of Cs[Ga:V]SH.[23] The spectra of Cs[Ga:V]SH suggest no deviation from trigonal symmetry, and this coincides with a very close match in the ionic radii of the gallium(III) and vanadium(III) cations.

EPR spectra of Cu(II) doped into various cubic oxide lattices, are well documented; and can usually be satisfactorily simulated assuming a simple Gaussian distribution in strain.[27] The spectra presented in this work are quite unique in that the distribution of species as a function of strain is certainly not continuous. Rather, there are islands of intensity [Fig. 2(c)] corresponding to certain magnitudes of the low symmetry perturbation. This correlates with there being more distortion coordinates of E_g symmetry for a hexa-aqua compared to hexa-oxo species. For the $[\mathrm{Ti(OH_2)_6}]^{3+}$ cation in Cs[Al:Ti]SH, there are five distortion coordinates of E_g symmetry (excluding the internal modes of the water molecule). This number is increased further if one includes the next coordination sphere, and, indeed there is strong evidence for significant coupling to a low energy phonon, which involves a displacement of the sulphate anion, coupled to the internal modes of the aqua ion.[6] In order for the larger titanium(III) cation to be accommodated into CsAlSH, the lattice clearly has to relax, and the EPR spectrum is a reflection of the statistical distribution of $[\mathrm{Ti(OH_2)_6}]^{3+}$ species. The manner in which the $[\mathrm{Ti(OH_2)_6}]^{3+}$ cation is accommodated will be influenced by local strains in the crystal. It is not surprising, therefore, that there is some variation in the EPR spectrum from crystal to crystal, and a strong dependence on how the sample is prepared.

The experimental contours in Fig. 2(c) are asymmetric, strewn out along the direction of the plot of JTB, which is consistent with the interpretation that the inhomogeneous broadening of the EPR lines results from a distribution of species subject to slightly different magnitudes of low symmetry strain. The general form of the CW spectra can be understood within this framework. Figure 7(a) presents simulated EPR spectra calculated with the same set of ligand field and vibronic coupling parameters used to calculate plot JTB. As described in Sec. III, the spectra were calculated as a superposition of EPR spectra arising from titanium(III) species subject to varying amounts of low symmetry strain. The height of the simulated EPR line decreases, and the linewidth increases, rapidly with increasing θ, in accordance with the experimental spectra. This occurs because $g_{\perp}$ increases to first-order in e_{θ}, and $g_{\|}$ only to second-order. Thus, the superposition of EPR resonances arising from species with a range of e_{θ} values, gives rise to a larger spread in $g_{\perp}$ compared to $g_{\|}$.

The angular dependence of the EPR spectra obtained from crystal Cs[Al:Ti]SH_B, presented in Fig. 4, cannot be reproduced assuming a simple Gaussian distribution in the parameter e_{θ}. Figure 7(b) is an attempt to simulate the EPR spectra by employing a double Gaussian distribution in e_{θ}. Although the two calculated Gaussian bands become better resolved as θ increases, the reproduction of the experimental spectrum is not satisfactory. Within the confines of our model, we have not been able to reproduce the asymmetric line shape at $\theta=0°$, and the pronounced splitting of the line with increasing θ. We have also tried varying the values of k and E_{JT} across the peak with little or no improvement. It is likely that our failure to simulate the data presented in Fig. 4

reflects our neglect of higher order terms. In the preceding analysis we have assumed an infinite trigonal field, in which case any deviation from trigonal symmetry may be described by one parameter. Dubicki and Riley have included the higher lying $^2A_g\,(S_6)$ trigonal term explicitly in their calculations, and have shown that even for a large trigonal field and a small low symmetry perturbation, there is a small, but non-negligible, dependence of the principal g values on the symmetry of the low symmetry distortion (see Fig. 5 in their paper).[5] Five parameters are required to describe the effect of a given low symmetry distortion on the energies of the states of the $^2T_g\,(T_h)$ ground term.[28] Our data suggest that there is a variation in the magnitude of strain across each peak, as seen most clearly in Fig. 2(c). In addition, there is likely to be a variation in the relative magnitudes of the five strain parameters in the array of titanium(III) species giving rise to each EPR line. The calculations of Dubicki and Riley suggest a complex interplay between the principle g values and the magnitude and symmetry of the distortion. This could give rise to the very peculiar line shapes, which we have observed. In addition, the relaxation times will vary across the EPR lines, which could distort the line shapes. A full and quantitative description would require expanding our electronic basis set to include the $^2A_g\,(S_6)$ trigonal term and calculating the angular dependence of the EPR spectra as a superposition of chemically distinct species, subject to distortions along different symmetry coordinates. In principal the structure of the complexes could be determined by ESEEM spectroscopy. However, we have undertaken angular overlap calculations, which suggest that a very small change in the $[Ti(OH_2)_6]^{3+}$ geometry is needed to produce a one-electron splitting of the $^2E_g\,(S_6)$ ground term of the magnitude suggested by our calculations.

Although there is little variation in the EPR spectra of different crystals of Cs[Al:Ti]SH, there is a significant change in a deuteriated sample, prepared under exactly the same conditions. The spectrum is shifted to higher g value, and this has been interpreted as resulting from a lower frequency of the Jahn-Teller active vibration.[6] Each resonance in the spectrum of Cs[Al:Ti]SH may be assigned a mean value of e_θ; and a corresponding peak is found in the deuteriated analogue for approximately the same value of e_θ. There is, however, a large difference between the spectra in terms of the intensities and linewidths of the resonances. This implies a different statistical distribution of titanium(III) species in the hydrated and deuteriated samples. The contrast between the spectra of Cs[Al:Ti]SH and Cs[Al:Ti]SD could be a consequence of small variations in the hydrogen bond strengths on account of the large change in the zero point energy of the O–H oscillators. The change in the linewidths and relative intensities of the EPR lines upon ^{18}O for ^{16}O substitution is far less significant; in this instance a significant change in hydrogen bonding would not be expected.

VI. CONCLUSION

This work provides overwhelming evidence in support of the interpretation that the anomalous EPR spectrum of Cs[Al:Ti]SH arises as a consequence of chemically distinct species, subject to varying amounts of low symmetry strain,

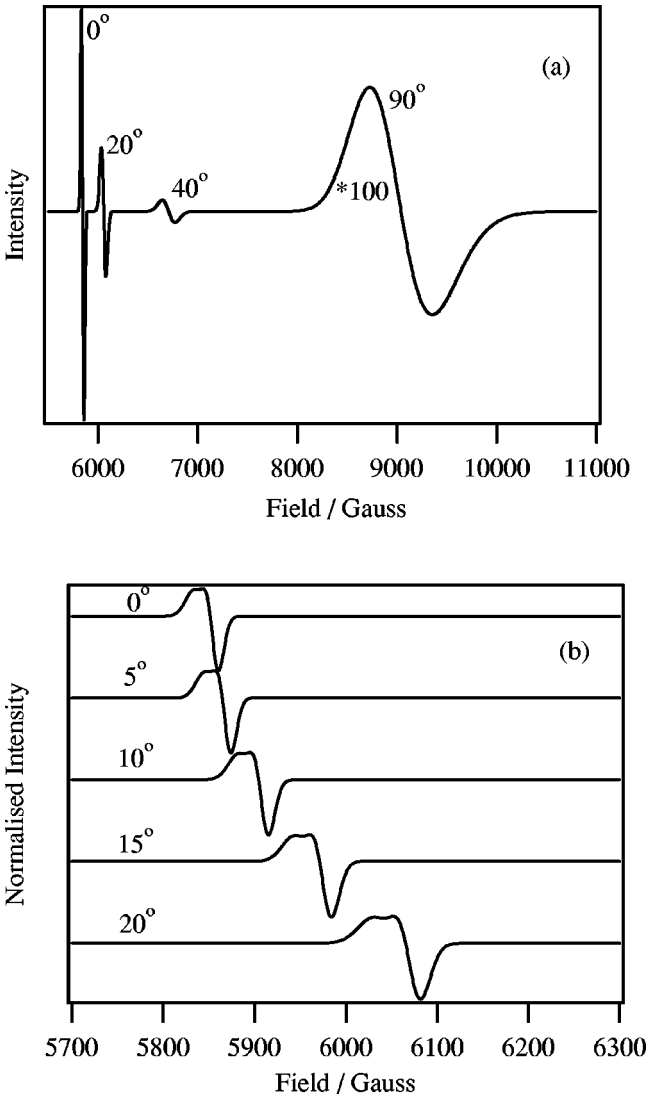

FIG. 7. (a) EPR simulations of an inhomogeneously broadened titanium(III) resonance, as a function of θ. The spectra were calculated using the following parameters: $\nu = 9.8$ GHz, $e_{\theta_m} = 8\ \mathrm{cm}^{-1}$, $e_{\theta_w} = 0.4\ \mathrm{cm}^{-1}$, and $\sigma = 4$ G. The vibronic Hamiltonian parameters are the same as those used to calculate plot JTB in Fig. 2(c). (b) EPR simulations of an inhomogeneously broadened titanium(III) resonance, as a function of θ. A double-Gaussian distribution in the strain parameter e_θ was assumed. For both Gaussian peaks, $\nu = 9.8$ GHz and $\sigma = 4$ G. For the low field peak $e_{\theta_m} = 8.18\ \mathrm{cm}^{-1}$, $e_{\theta_w} = 0.33\ \mathrm{cm}^{-1}$; for the high field peak $e_{\theta_m} = 7.82\ \mathrm{cm}^{-1}$ and $e_{\theta_w} = 0.23\ \mathrm{cm}^{-1}$. The high field peak was assigned an intensity 1.35 times greater than that for the low field peak. The vibronic Hamiltonian parameters are the same as those used to calculate plot JTB in Fig. 2(c).

as proposed by Dubicki and Riley.[5] Our work has utilised a new pulsed-EPR technique, which yields the $g_\parallel$ vs $g_\perp$ values for all lines in the complicated EPR spectrum, from just one crystal orientation. The advantage of the nutation experiment over conventional CW EPR, is that instead of a pair of g values for each line in the spectrum, a complete two-dimensional picture is produced. The spectrum graphically depicts the $g_\parallel$ vs $g_\perp$ relation; it also shows clearly that the origin of the large linewidths, observed for some of the EPR lines, is inhomogeneous broadening, which can be described adequately only in two dimensions. This is in contrast to the way inhomogeneous broadening is commonly perceived as a

one-dimensional distribution. Thus, this represents another example in which a two-dimensional spectrum, as determined by pulsed EPR, is far more informative than a conventional one-dimensional CW-spectrum. The nutation spectrum obtained is believed to be the first case in which a strain broadening interaction is shown in both $g_{\parallel}$ and $g_{\perp}$. It can be concluded that this technique will be important in characterizing similar systems, providing information that cannot be obtained from other techniques.

We suggest that the origin of the low symmetry interaction simply derives from a mismatch of the host and dopant ionic radii, and that the EPR spectra reflect the various ways of accommodating the $[Ti(OH_2)_6]^{3+}$ cation in the CsAlSH lattice. The calculated $g_{\parallel}$ vs $g_{\perp}$ relation is very sensitive to the effective frequency of the Jahn-teller active mode, and a satisfactory reproduction of the experimental data is obtained by assuming a vibronic coupling model in accordance with that employed to model the susceptibility data.[6] Furthermore, we have been able to provide a reasonable estimate of the one-electron splitting of CsTiSH, which results from the 12 K phase transition.[8] Both the nature of the electron–phonon interaction, and the magnitude of the one-electron splitting, are central to understanding the nature of the cooperative Jahn-Teller interaction.[29]

The model that we have employed to explain the nutation spectrum also accounts for the general anomalous features of the CW spectra, i.e., the pronounced broadening of some of the EPR lines with increasing θ. However, the observed splitting of some of the lines with increasing θ, cannot be explained within the confines of our model. Further experimental and theoretical work is required to provide a complete description of this fascinating and instructive system.

ACKNOWLEDGMENTS

This work was funded by the Swiss National Science Foundation, the Royal Society, and the Australian Research Council. We thank Graham Hanson for the use of the *S*-band EPR spectrometer, and Anne-Laura Barra for technical assistance in obtaining *W*-band spectra at the Grenoble high magnetic field laboratory, France. We are also indebted to Alexander Weixelbaumer, who performed the elemental analysis on our crystals.

[1] G. A. Woonton and J. A. Mackinnon, Can. J. Phys. **46**, 59 (1968).
[2] A. Manoogian, Can. J. Phys. **48**, 2577 (1970).
[3] G. F. Dionne, Can. J. Phys. **50**, 2232 (1972).
[4] Y. H. Shing and D. Walsh, Phys. Rev. Lett. **33**, 1067 (1974).
[5] L. Dubicki and M. J. Riley, J. Chem. Phys. **106**, 1669 (1997).
[6] P. L. W. Tregenna-Piggott, M. C. M. O'Brien, J. R. Pilbrow, H-U. Güdel, S. P. Best, and C. Noble, J. Chem. Phys. **107**, 8275 (1997).
[7] R. L. Carlin, *Magnetochemistry* (Springer-Verlag, Berlin, 1986).
[8] P. L. W. Tregenna-Piggott, S. P. Best, M. C. M. O'Brien, K. S. Knight, J. B. Forsyth, and J. R. Pilbrow, J. Am. Chem. Soc. **119**, 3324 (1997).
[9] S. P. Best and J. B. Forsyth, J. Chem. Soc. Dalton Trans. **1991**, 1721.
[10] P. L. W. Tregenna-Piggott and S. P. Best, Inorg. Chem. **35**, 5730 (1996).
[11] P. L. W. Tregenna-Piggott, M. C. M. O'Brien, H. Weihe, and H. U. Güdel, J. Chem. Phys. **109**, 2967 (1998).
[12] S. P. Best, J. K. Beattie, and R. S. Armstrong, J. Chem. Soc. Dalton Trans. **1984**, 2611.
[13] F. Muller, A. Hopkins, N. Coron, M. Grynberg, L. C. Brunel, and G. Martinez, Rev. Sci. Instrum. **60**, 3681 (1989); A. L. Barra, L. C. Brunel, and J. B. Robert, Chem. Phys. Lett. **165**, 107 (1990).
[14] M. Willer and A. Schweiger, Chem. Phys. Lett. **264**, 1 (1996).
[15] T. Takui, K. Sao, D. Shiomi, K. Itoh, T. Kaneko, E. Tschchida, and H. Hishide, Mol. Cryst. Liq. Cryst. **279**, 155 (1996).
[16] Y. C. Zhong and J. R. Pilbrow, Chem. Phys. Lett. **222**, 592 (1994).
[17] J. Isoya, H. Kanda, and Y. Uchida, Phys. Rev. B **42**, 9843 (1990).
[18] S. Stoll, G. Jeschke, M. Willer, and A. Schweiger, J. Magn. Reson. **130**, 86 (1998).
[19] R. Song, Y. C. Zhong, C. J. Noble, J. R. Pilbrow, and D. R. Hutton, Chem. Phys. Lett. **243**, 324 (1995).
[20] F. G. Anderson, F. S. Ham, and G. D. Watkins, Phys. Rev. B **45**, 3287 (1992).
[21] F. S. Ham, Phys. Rev. **138**, A1727 (1965); Phys. Rev. **166**, 307 (1968).
[22] P. L. W. Tregenna-Piggott, S. P. Best, H. U. Güdel, H. Weihe, and C. C. Wilson, J. Solid State Chem. **145**, 460 (1999).
[23] P. L. W. Tregenna-Piggott, H. Weihe, J. Bendix, A.-U. Barra, and H. U. Güdel, Inorg. Chem. **38**, 5928 (1999).
[24] B. Bleaney, G. S. Bogle, A. H. Cooke, R. J. Duffus, M. C. M. O'Brien, and K. W. H. Stephens, Proc. Phys. Soc., London, Sect. A **68**, 57 (1955).
[25] L. L. Chase, T. J. Glynn, W. Hayes, A. J. Rushwork, J. F. Ryan, D. Walsh, and A. M. Goer, in *Proceedings of the Fifth International Conference on Raman Spectroscopy*, Freiburg, Germany, 1976, edited by E. D. Schmid, J. Brandmueller, and W. Kiefer (Hans Ferdinand Schulz, Berlin, 1976), pp. 660–661.
[26] P. L. Tregenna-Piggott and H. U. Güdel (in preparation).
[27] R. W. Reynolds and L. A. Boatner, Phys. Rev. B **12**, 4735 (1975).
[28] The five parameters could be reduced to effectively four, by taking appropriate linear combinations of the strain tensors transforming as T_{yz}, T_{xz}, and T_{xy} and absorbing the parameter which multiplies the matrix transforming as $1/\sqrt{3}(T_{yz}+T_{xz}+T_{xy})$ into the trigonal field.
[29] G. A. Gehring and K. A. Gehring, Rep. Prog. Phys. **38**, 1 (1975); M. D. Kaplan and B. G. Vekhter, *Cooperative Phenomena in Jahn-Teller Crystals* (Plenum, New York, 1995).